INSTITUTE OF PLASMA PHYSICS

NAGOYA UNIVERSITY

PLASMA HEATING, CONFINEMENT AND STABILIZATION EXPERIMENTS IN AXISYMMETRIC MIRROR-CUSP DEVICE

S. Okamura, R. Kumazawa, K. Adati, T. Aoki, H. Fujita, K. Hattori, S. Hidekuma, T. Kawamoto, Y. Okubo, T. Sato, T. Hatori, K. Muraoka, K. Uchino, M. Maeda, M. Hamamoto, K. Sunako, K. Takayama, D.R. Baker, H.R. Garner, H.D. Price, P.B. Parks, A.M. Sleeper, R. Itatani, Y. Yasaka

(Received July 31, 1984)

IPPJ-690 Aug. 1984

RESEARCH REPORT

NAGOYA, JAPAN

PLASMA HEATING, CONFINEMENT AND STABILIZATION EXPERIMENTS IN AXISYMMETRIC MIRROR-CUSP DEVICE*,**

S. OKAMURA, R. KUMAZAWA, K. ADATI, T. AOKI H. FUJITA, K. HATTORI, S. HIDEKUMA, T. KAWAMOTO, Y. OKUBO, T. SATO, T. HATORI, K. MURAOKA***, K. UCHINO***, M. MAEDA†, M. HAMAMOTO††, K. SUNAKO†††, K. TAKAYAMA†††, D.R. BAKER§, H.R. GARNER§, H.D. PRICE§, P.B. PARKS§, A.M. SLEEPER§, R. ITATANI§§, Y. YASAKA§§

(Received - July. 31, 1984)

IPPJ- 690 Aug. 1984

Further communication about this report is to be sent to the Research Information Center, Institute of Plasma Physics, Nagoya University, Nagoya 464, Japan.

---

* Preprint for IAEA 10th Int. Conf. Plasma Physics and Controlled Thermonuclear Fusion Research, London 1984

** Work supported in part by the United States Department of Energy

*** Kyushu University, Kasuga Fukuoka, Japan

† Kyushu University, Hakozaki, Fukuoka, Japan

†† Oita University, Oita, Japan

††† Tokai University, Hiratsuka, Japan

§ GA Technologies Inc., San Diego, California, USA

§§ Kyoto University, Sakyo-ku, Kyoto, Japan

Abstract

This paper describes recent experimental results of ICRH plasma production, RF plugging and ambipolar potential plugging in RFC-XX-M (IPP, Nagoya). Results of ICRF heating and RF stabilization in HIEI (Kyoto) are also described.

1. INTRODUCTION

Axisymmetricity is an important issue to suppress the radial transport in linear confinement systems. The RFC-XX-M device has a linear, axisymmetric MHD stable configuration which is a simple mirror field terminated by spindle cusp fields with radio-frequency (RF) plugging. HIEI is also an axisymmetric mirror machine in which MHD stability is achieved by RF stabilization.

In RFC-XX-M, plasma confinement with RF plugging was greatly improved since the last conference. Joint JAPAN/U.S. cooperation to investigate the ambipolar potential plugging in RFC-XX began in 1982 resulting in an increase in axial confinement time also. In HIEI, ICRF heating for a deuterium-hydrogen plasma was carried out. The mechanism of RF stabilization for MHD mode was clarified.

2. EXPERIMENTS ON RFC-XX-M

2.1 ICRH Sustained Plasma

A schematic diagram of RFC-XX-M is shown in Fig. 1. The distance between the field-null points is 3 m. The magnetic field strength of the central mirror is 0.35 T at the midplane and 0.96 T at the throat. To produce plasmas, a rotating type-

III antenna [1] is installed at the mirror throat and is excited by two 0.4-MW RF oscillators. We can excite the m=-1 mode (left-handed rotating), the m=+1 mode (right-handed rotating), or the m=±1 mode (non-rotating).

An initial seed plasma is injected externally or produced by ECRH (2.45 GHz) in the field-null region. After the partial decay of the seed plasma, the rotating type-III antenna is excited coincident with hydrogen gas puffing. The frequency is 7 MHz which corresponds to ω/ω_{ci} at the antenna of 0.48 to 0.97 when the magnetic field is varied from 100 % to 50 %. For m=-1 mode, the radial density profile is nearly flat with the magnitude of 10^{13} cm^{-3} for net RF input power of 100 kW. The ion (perpendicular) temperature can be varied between 100 and 500 eV by changing RF power. The electron temperature changes from 10 to 30 eV. The on-axis neutral density is less than 1×10^{10} cm^{-3}, so that charge-exchange energy loss is not dominant. For m=+1 mode, the radial profile has a sharp on-axis peak of 7×10^{13} cm^{-3} and the ion temperature is about 50 eV.

In RFC-XX-M the entire plasma is stabilized by the favorable curvature of the cusp field. We do not observe unstable activity for the standard operation except for the case with reduced gas puffing which makes the pressure ratio of the cusp plasma to the central mirror plasma smaller than a threshold. In this case the plasma stability can be regained by additional gas puffing only in the cusp region to increase the cusp plasma pressure.

The confinement of the hotter plasma produced with the m=-1 mode has been investigated without RF plugging. The energy confinement time τ_E is measured by the decay time of the midplane diamagnetic loop signal. In Fig. 2, τ_E is plotted in the function of the on-axis perpendicular ion temperature $T_{i\perp}$ measured with the diamagnetic loop and the neutral particle energy analyzer. The electron drag time τ_d is evaluated from the spatial distribution of the electron temperature measured by Thomson scattering taking account of the profile of electron density. The charge exchange time τ_{cx} is also estimated based on the neutral hydrogen density measurement by the laser fluorescent method [2]. From the relation $1/\tau_E = 1/\tau_d + 1/\tau_{cx} +$

$1/\tau_E^p$, where $1/\tau_E^p = 1/\tau_{E//} + 1/\tau_{E\perp}$, we estimate the energy confinement time due to particle loss τ_E^p. Values of τ_E^p have been in the range of 0.2 to 2 ms for $T_{i\perp}$ = 100 - 500 eV.

2.2. RF Plugging

The entire plasma in the region between two line cusps including the central mirror is confined by RF plugging in both line cusps. The plugging RF is applied to a pair of ring electrodes installed in each line cusp. The frequency is 24.5 MHz which gives $\omega/\omega_{ci} \sim 1.1$. With the RF plug to both line cusps, the total energy confinement is improved to τ_E = 1.1 ms with $n = 6 \times 10^{12}$ cm^{-3}, $T_{i\perp}$ =380 eV and T_e = 46 eV. For this case, we obtain estimations of τ_d = 2 ms and τ_{cx} = 3 - 4 ms which give $\tau_E^p \sim 10$ ms (within a factor of 2).

In order to measure the RF plug potential directly, a series of experiments have been carried out using multigrid energy analyzers (MGA) set up around the line cusp end wall and emissive probes inserted near the RF electrodes. Figure 3 shows the MGA current voltage curve for the case of a single line cusp plugging. The knee of the curve gives the sum of the RF plug potential ψ and the plasma potential ϕ_p in the plug region. When the RF plugging is applied only at the LS line cusp, the potential $\psi + \phi_p$ measured by the LS MGA increases remarkably, while the value measured at the LB MGA increases little. The RF plug potential is given approximately by the difference in potentials measured by the LS MGA and the LB MGA as depicted in Fig 3. Values of ψ are plotted against ω/ω_{ci} in Fig. 4(a). This shows that ψ can be produced for $\omega/\omega_{ci} > 1$. This is consistent with the dispersion relation of the eigenmode of electrostatic waves.

The plasma potential at the plug can be directly measured by an emissive probe in the LS plug section. Typical values of ϕ_p range from 85 to 130 V when the plug RF voltage are varied up to 1.8 kV. Subtracting ϕ_p from the potential measured by the MGA, one can obtain ψ. Figure 4(b) shows that ψ is nearly proportional to V^2_{plug} as expected from the theory.

2.3. Ambipolar Plugging

RFC-XX-M has been operated as an ambipolar plugged tandem mirror. This is done by fueling the cusp end cells with hydrogen gas to build high densities. No RF plugging is used. In this mode the cusp end cells function of both the anchor and plug functions. Since no thermal barriers are present electrons heated either by drag from the ions or directly from the ICRH ionize the injected gas in the cusp. As ICH beaches exist on the inboard and outboard sides of the cusp anchors, the possibility exists that some heating/trapping of ions is done there.

The time history of a shot with end cell gas puffing is shown in Fig. 5. Startup is from 2.5 ms to 6 ms. ICH and central cell gas puffing sustain the plasma from 6 ms for 12 ms. After the turn on of the ICH (at 2 ms) end cell gas puffing is begun. An equilibrium is reached and maintained with $n_{ec}/n_{cc} \sim 3.3$.

Typical plasma parameters in the ambipolar plugging mode are $n_{cc} \sim 5 \times 10^{12}$ cm^{-3}, $T_{i\perp} \sim 250$ eV and $T_e \sim 25$ eV. The axial density profile of this mode is shown in Fig. 6 before and after end cell gas puffing. Even without end cell puffing, RFC-XX-M is MHD stable with end cell pressure considerably less than center cell pressure due to the strong curvature in the cusp end cell. For $n_{ec}/n_{cc} \sim 2$, the resulting plugging potential is about 50 eV. In general the plugging potential is higher than that predicted by the Boltzmann relation.

The axial confinement time of the entire plasma (determined as the ratio of the total number of confined particles to the total end loss flux) increases by a factor of 3 - 5 over that for the standard operating mode. During ambipolar plugging the central cell density increases. The time evolution of the central cell radial density profile suggests that the ambipolar plugging potential peaks radially on axis. Confinement of near-axis particles (which otherwise may be nonadiabatic) is improved most. Thomson scattering electron temperature measurements demonstrate that when end cell puffing starts the on-axis electron temperature is depressed but then recovers its initial value within 3 ms.

During ambipolar plugging the spectra of density and floating potential fluctuations in the central cell was obtained. Modes tentatively identified as density gradient drift waves propagating in the electron drift direction were observed with $\tilde{n}/n \approx 5\%$, $\tilde{\phi}/T_e \sim 50\%$, and $\omega \sim \frac{1}{5}\omega_e^* \sim 6 \times 10^4\ s^{-1}$. The maxima in $\tilde{n}$ and $\tilde{\phi}$ occur near the maximum density gradient. The calculated upper bound on the radial diffusion coefficient arising from these fluctuatons is $D_\perp \sim 1\times10^4\ cm^2/s$. The fluctuation levels are decreased by at least 50% in this high end cell density mode compared to those in low density mode.

3. FAST WAVE HEATING AND STABILIZATION IN HIEI

In HIEI deuterium plasma with (10-30)% of hydrogen concentration or pure hydrogen plasma of density $n \approx (10^{13}\text{-}10^{14})$ cm^{-3} is produced in a static magnetic field up to 1.1 T at the throat. The length between the mirror points is 1.2 m and the mirror ratio R is variable from 1.4 to 4.

The RF antenna at the throat produces circularly or linearly polarized fields of $|m| = 1$ mode in line-tied D + H plasma. Fast waves of $k \lesssim 10\ m^{-1}$ were observed to propagate towards the midplane for linearly and right-hand circularly polarized excitation with $\omega/\omega_{cD} > 1$. No wave was found for left-hand polarized excitation. Figure 7(a) shows the phase difference of the wave magnetic field along the axis obtained from the experiment and cold plasma theory with WKB approximation for R = 1.5 and $\omega/\omega_{cD} = 3$ at the throat.

The increment of $nT_{i\perp}$ is plotted in Fig. 7(b) as a fuction of ω/ω_{cH} at the throat. For H plasma, the heating may be due to collisional effect and small left-hand polarized component of partially excited slow wave near the periphery. For D + H plasma, large increase of $nT_{i\perp}$ is observed when the ion-ion hybrid resonance zone lies inside the throat. The maximum heating rate was $\sim 1.2 \times 10^{13}$ $eVcm^{-3}/kW$ for $\omega/\omega_{cH} = 0.95$.

When the line-tying is removed, the plasma becomes flute-unstable and the RF heating is very inefficient. This shows that the RF field of $|m| = 1$ mode cannot produce the

ponderomotive force to oppose the effective gravity. The stability is achieved when the m = ±2 RF field is further applied by the midplane antenna [3]. Figure 8(a) shows the measured radial distribution of the RF magnetic field at the midplane with which the flute instability is stabilized in H plasma. The solid curves denote the self-consistent RF fields in a diffuse-boundary cold plasma obtained from Hojo and Hatori's RF code. The radial ponderomotive force for ions for this RF field is calculated in Fig. 8(b). Measured fluctuation amplitudes of flute mode with and without the midplane RF is compared with the result of Hojo's stability code in Fig. 8(c). The eigenfunction of the dispersion relation of flute mode [4] with (solid line) and without (dotted line) the ponderomotive force shown in Fig. 8(b) is plotted. The good agreement between the experiment and the calculation leads to the conclusion that the ponderomotive force is essential for the stabilization of flute mode.

ACKNOWLEDGEMENTS

The authors would like to express their gratitude to Prof. H. Kakihana, the former director of the Institute of Plasma Physics, Dr. T. Ohkawa and Dr. R.L. Freeman for their continuous encouragement. We also wish to acknowledge stimulating discussions with Prof. J.H. Malmberg, and collaboration of Dr. H. Hojo using his computer codes.

REFERENCES

[1] WATARI, T., et al., Nucl. Fusion 22 (1983) 1359.
[2] MURAOKA, K., et al., Proc. 6th Int. Conf. Plasma Surface Interactions in Controlled Fusion Devices, Nagoya, 1984.
[3] INUTAKE, M., et al., Plasma Phys. and Controlled Nucl. Fusion Research (Proc. 9th Int. Conf., Baltimore, 1982) Vol.1, IAEA, Vienra (1983) 545.
[4] ROSENBLUTH, M. and SIMON, A., Phys. Fluids 8 (1965) 1300.

Figure Captions

Fig. 1 Schematic drawing and diagnostic system of RFC-XX-M.

Fig. 2 Dependence of τ_E, τ_{cx}, τ_d and τ_E^p on ion temperature.

Fig. 3 Current-voltage characteristics of MGA measured at the LS and the LB line cusps when RF plugging is applied only at the LS line cusp.

Fig. 4 (a) ψ versus ω/ω_{ci}. (b) ψ versus plug RF voltage V_{plug}.

Fig. 5 Typical data for a shot with end cell gas puffing.

Fig. 6 Axial density profiles with and without end cell gas puffing.

Fig. 7 (a) Phase difference of fast wave along the axis obtained experimentally (circles) and theoretically (solid line). (b) Heating rate versus ω/ω_{cH} at the throat.

Fig. 8 (a) Measured and calculated wave magnetic field versus r for $n = 5 \times 10^{13}$ cm^{-3} and $\omega/\omega_{cH} = 2.4$. (b) Radial ponderomotive force for ions for the wave field in (a). (c) Measured and calculated amplitudes of the flute fluctuation.

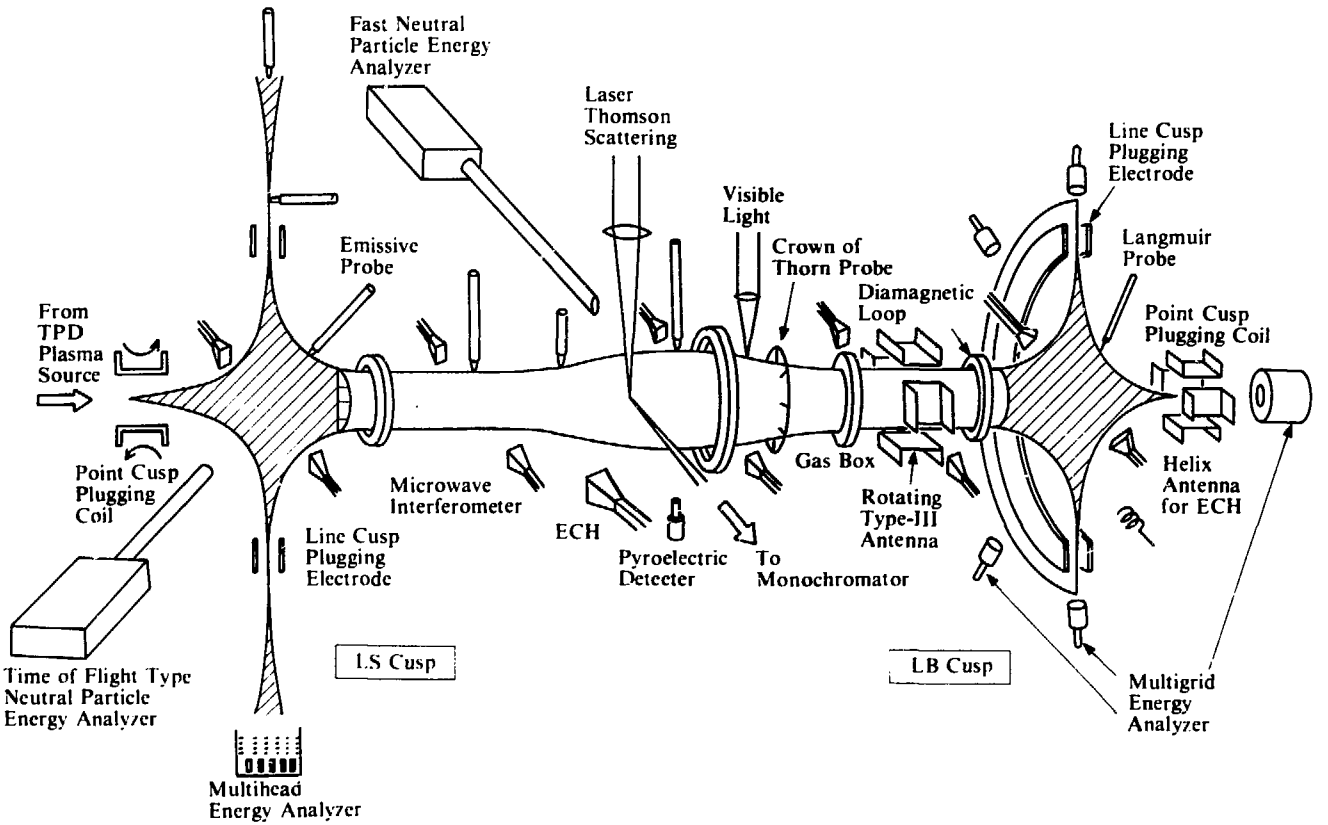

Fig. 1 Schematic drawing and diagnostic system of RFC-XX-M.

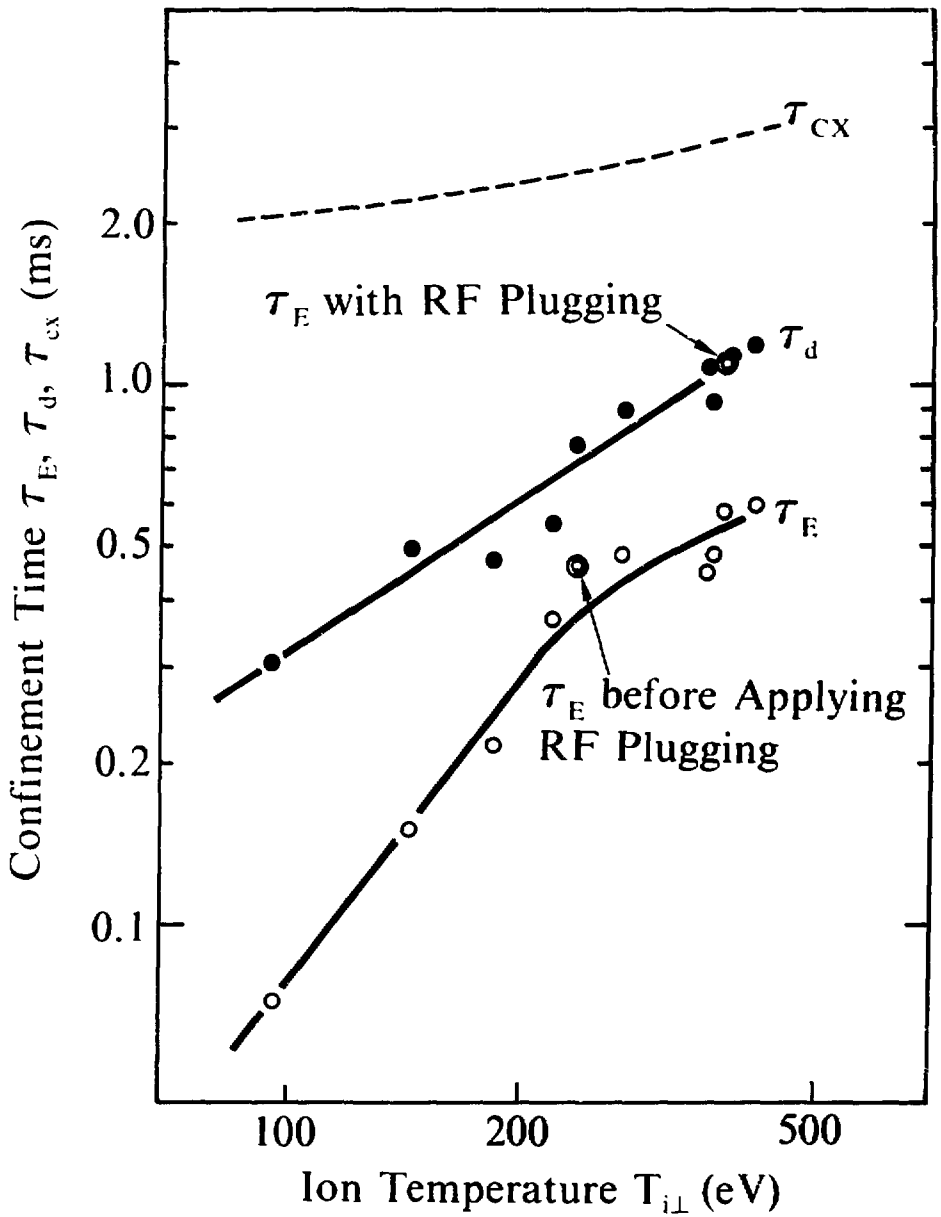

Fig. 2 Dependence of τ_E, τ_{cx}, τ_d and τ_E^p on ion temperature.

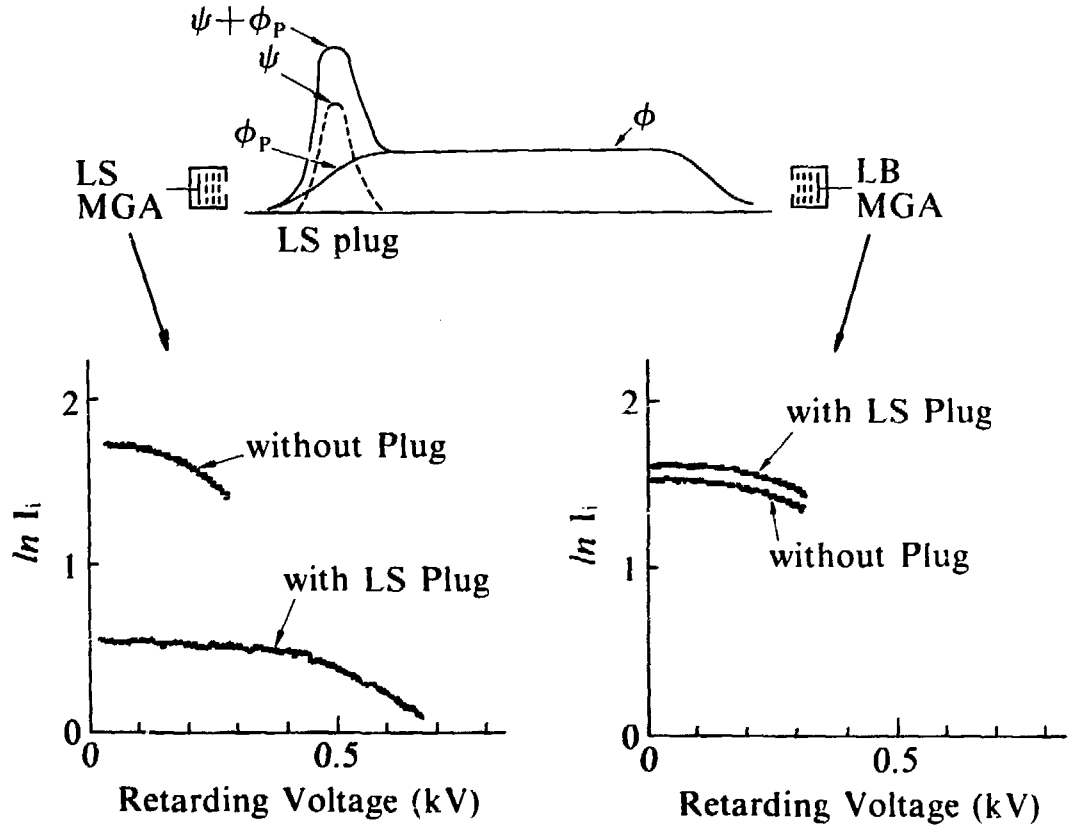

Fig. 3 Current-voltage characteristics of MGA measured at the LS and the LB line cusps when RF plugging is applied only at the LS line cusp.

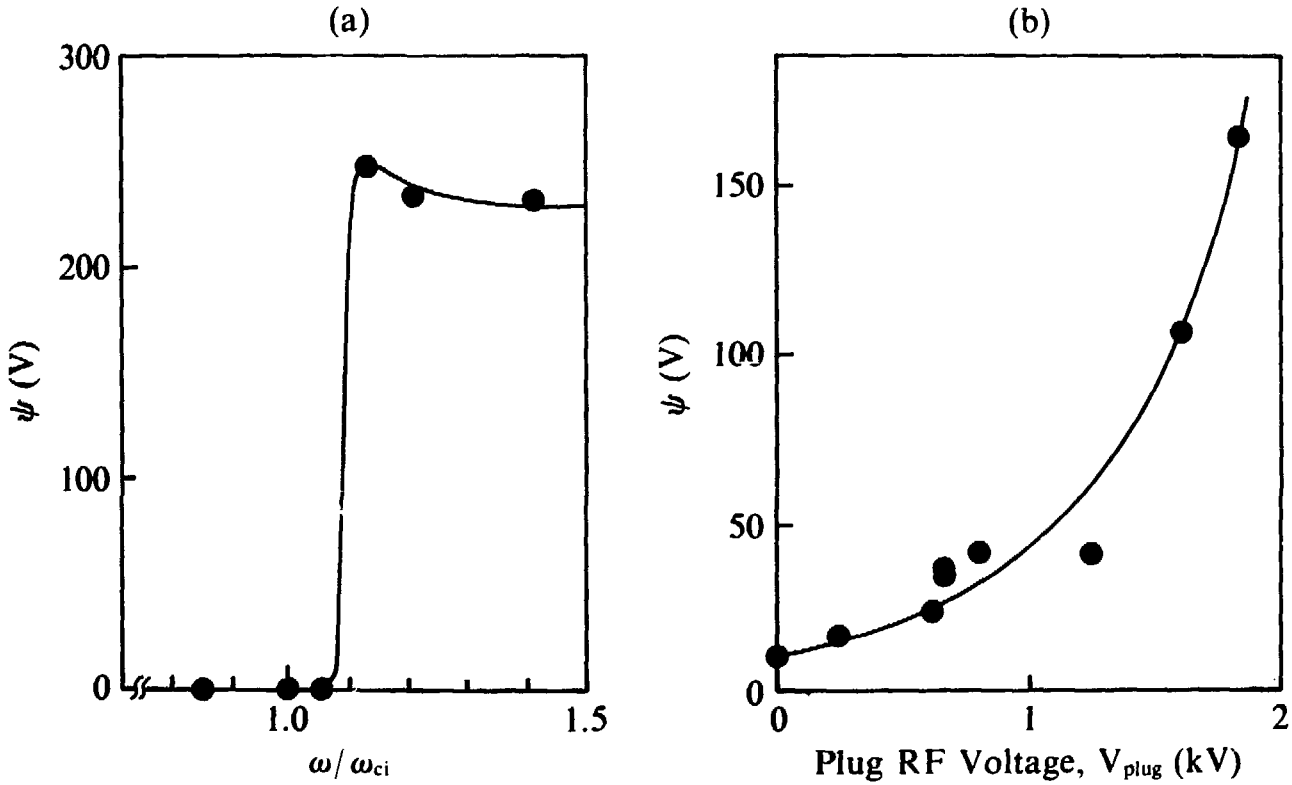

Fig. 4 (a) ψ versus ω/ω_{ci}. (b) ψ versus plug RF voltage V_{plug}.

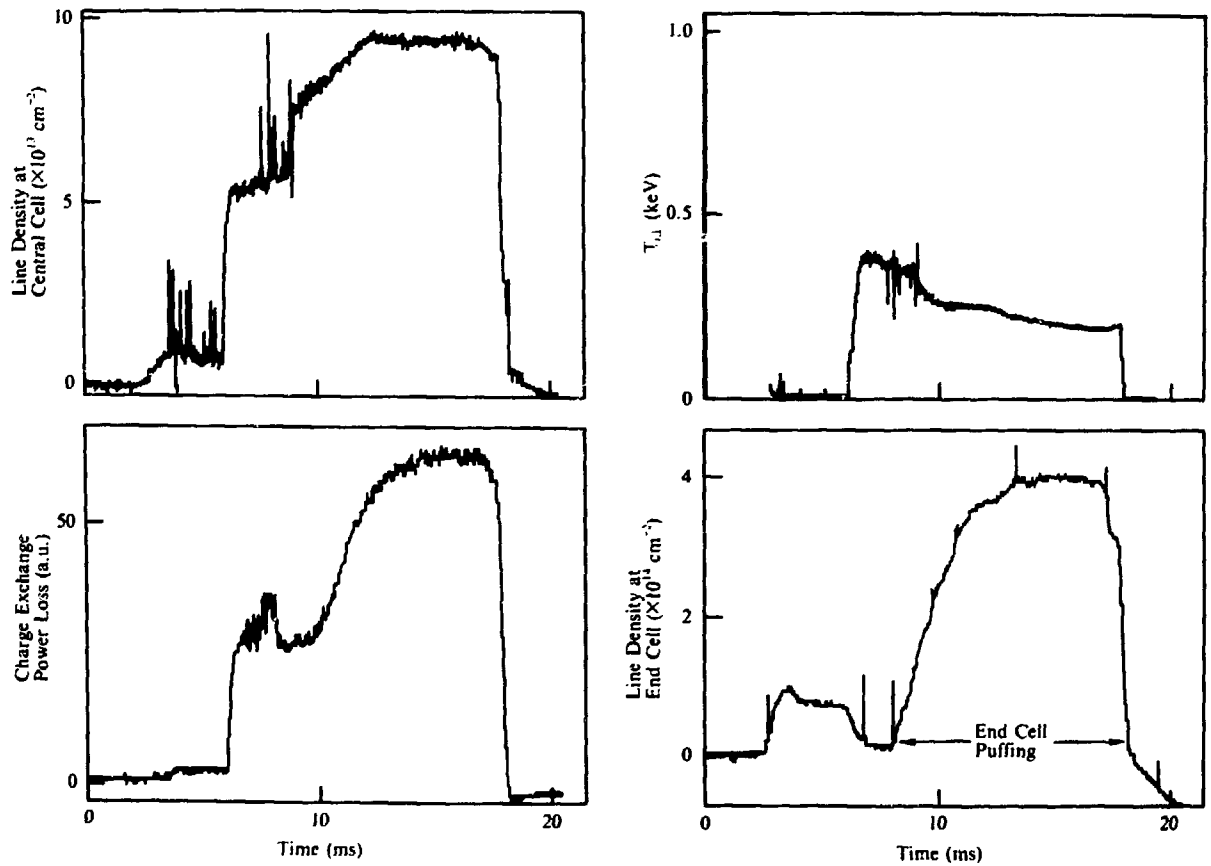

Fig. 5 Typical data for a shot with end cell gas puffing.

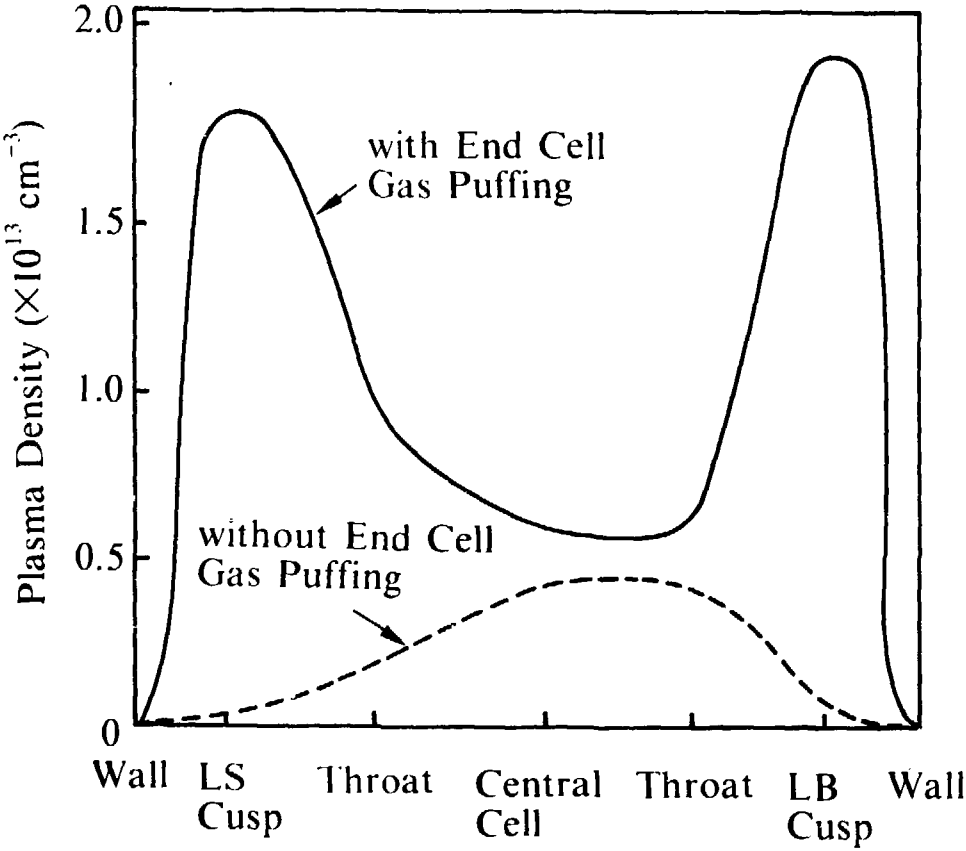

Fig. 6 Axial density profiles with and without end cell gas puffing.

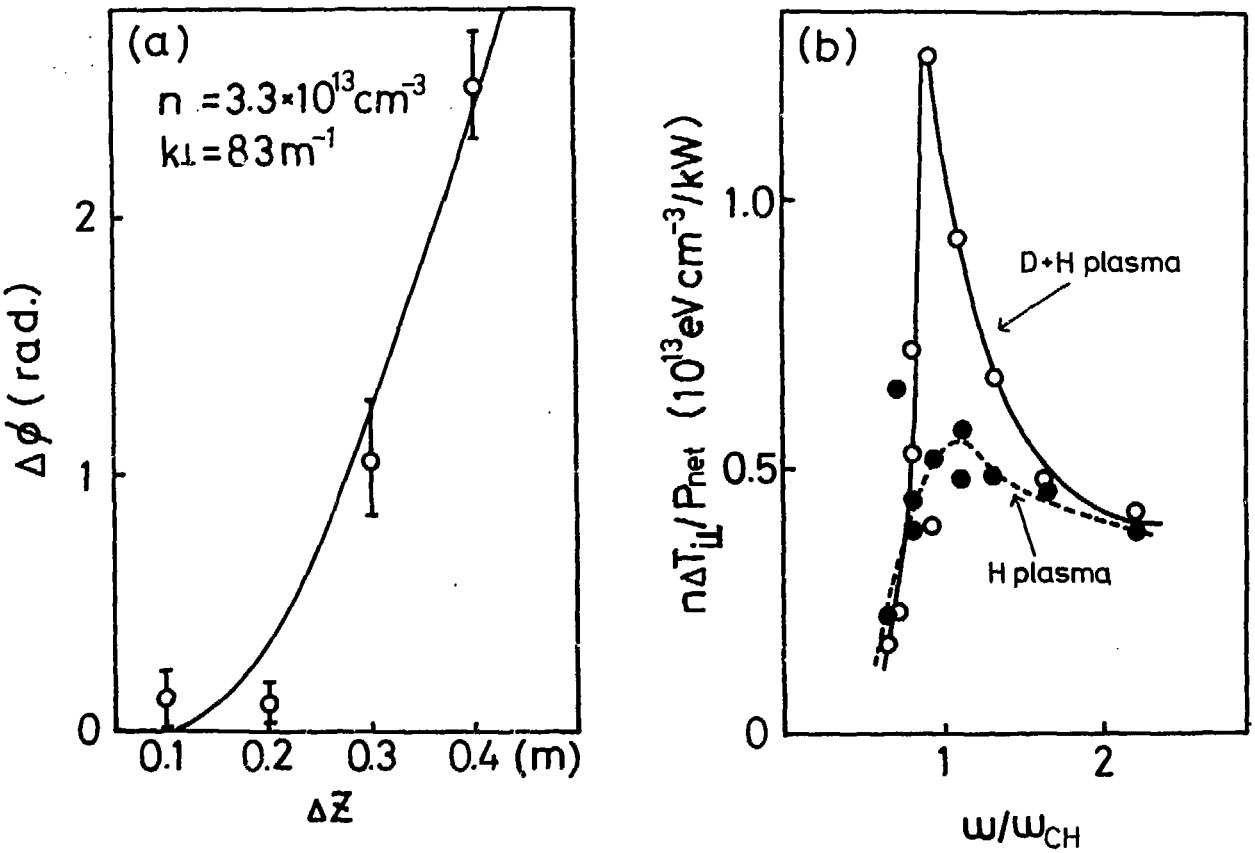

Fig. 7 (a) Phase difference of fast wave along the axis obtained experimentally (circles) and theoretically (solid line). (b) Heating rate versus ω/ω_{cH} at the throat.

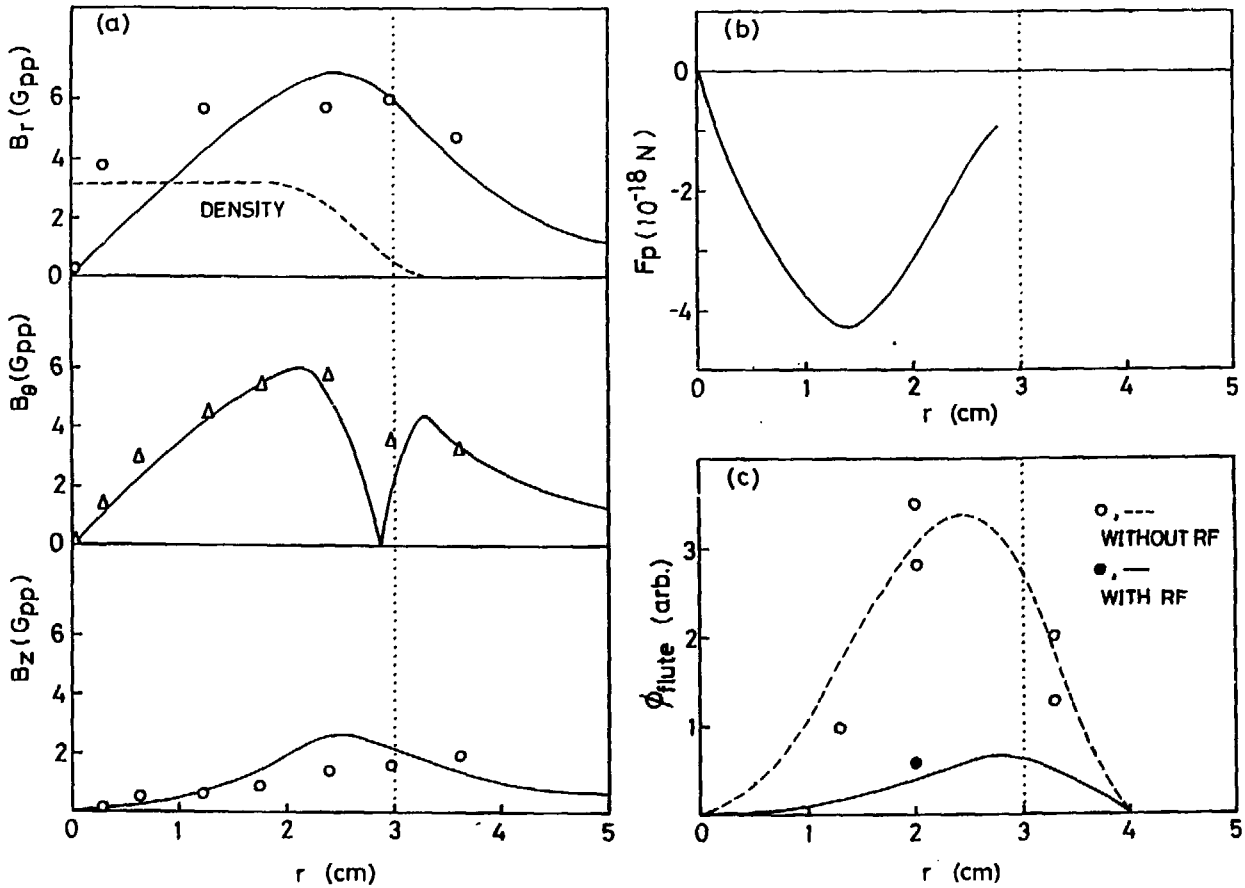

Fig. 8 (a) Measured and calculated wave magnetic field versus r for $n = 5 \times 10^{13}$ cm^{-3} and $\omega/\omega_{cH} = 2.4$. (b) Radial ponderomotive force for ions for the wave field in (a). (c) Measured and calculated amplitudes of the flute fluctuation.